Multivalent ion–DNA interaction: Neutron scattering estimates of polyamine distribution

S. S. Zakharova, S. U. Egelhaaf, L. B. Bhuiyan, C. W. Outhwaite, D. Bratko et al.

Citation: J. Chem. Phys. **111**, 10706 (1999); doi: 10.1063/1.480425
View online: http://dx.doi.org/10.1063/1.480425
View Table of Contents: http://jcp.aip.org/resource/1/JCPSA6/v111/i23
Published by the American Institute of Physics.

Multivalent ion–DNA interaction: Neutron scattering estimates of polyamine distribution

S. S. Zakharova
Leiden Institute of Chemistry, Gorlaeus Laboratories, Leiden University, P.O. Box 9502, 2300 RA Leiden, The Netherlands

S. U. Egelhaaf
Department of Physics, JCMB, University of Edinburgh, Edinburgh EH9 3JZ, United Kingdom

L. B. Bhuiyan
Laboratory of Theoretical Physics, Department of Physics, Box 23343, University of Puerto Rico, Rio Piedras, Puerto Rico 00931-3343

C. W. Outhwaite
School of Mathematics, University of Sheffield, Sheffield S3 7RH, United Kingdom

D. Bratko
College of Chemistry, University of California, Berkeley, California 94720

J. R. C. van der Maarel[a)]
Leiden Institute of Chemistry, Gorlaeus Laboratories, Leiden University, P.O. Box 9502, 2300 RA Leiden, The Netherlands

(Received 31 August 1999; accepted 22 September 1999)

The partial structure factors pertaining to DNA–DNA, DNA–polyamine, and polyamine–polyamine density correlations in DNA fragment (contour length 54 nm) solutions have been measured with small angle neutron scattering and contrast matching in water. The effect of the polyamines putrescine and spermidine on the DNA molecular structure is gauged from the limiting behavior of the DNA–DNA partial structure factor at high values of momentum transfer. The double layer structure and the extent to which the polyamines can approach the DNA are derived from the DNA–polyamine and polyamine–polyamine partial structure factors. For this purpose, the structure factors are interpreted with the correlation functions derived from the classical Poisson–Boltzmann and the modified Poisson–Boltzmann equations and/or Monte Carlo simulation. For simple salt free DNA with tetramethylammonium or putrescine counterions, spatial fluctuations in the charge density are discussed in terms of the charge structure factor. The structural arrangement of putrescine and spermidine can be fully rationalized in terms of their valence. In the case of spermidine, it is necessary to include ionic correlation effects, but this could be accomplished by modeling the ligands as hard spheres. The polyamines have no detectable effect on the DNA molecular structure and are too large to penetrate the grooves to any significant extent. These results imply that DNA condensation in the presence of polyamines is largely governed by electrostatic interactions, rather than by the binding of the multivalent cation *per se*. © *1999 American Institute of Physics.* [S0021-9606(99)50847-7]

I. INTRODUCTION

In biological systems, DNA is often very tightly packed with concentrations up to 400 mg/ml. The structural organization is largely unknown, but bears some resemblance to condensed DNA phases observed *in vitro*. Model systems that can produce condensed DNA phases are of great interest for understanding the mechanisms involved *in vivo*. An important experimental approach is DNA condensation induced by condensing agents, e.g., polyamines of valence 3 or greater, polypeptides, and/or proteins.[1,2] Polyamines are found in all bacteria and most animal cells. They are growth factors and they serve to stabilize the structure of membranes, ribosomes, and some viruses.[3] Although much work has been done to elucidate the mechanisms involved in stabilizing the condensed state, the structural arrangement of the condensing agents near DNA is not clear.[2,4,5]

Detailed structural information can be inferred from small angle neutron (SANS) or x-ray (SAXS) scattering. The scattering is sensitive to the set of spatial Fourier transforms of the solute density correlation functions, i.e., the partial structure factors.[6] Chen and co-workers have investigated the distribution of heavy metal Cs^+ and Tl^+ about DNA and cylindrical micelles with SAXS.[7–9] Recently, similar experiments were reported for I^- counterions around a cationic polyelectrolyte with a rodlike poly(*p*-phenylene) backbone.[10] The intensities compared favorably with the relevant *combination* of partial structure factors derived from the classical Poisson–Boltzmann (PB) theory. The potential of the SANS approach lies in its spatial resolution together with contrast

a)Author to whom correspondence should be addressed.

variation to blank or highlight certain components in a complex mixture of DNA, solvent, counter- and co-ions, and ligands. SANS methods based on variation of the isotopic composition of the solvent have made it possible to determine *individual* polyion–polyion, polyion–counterion, and counterion–counterion partial structure factors in solutions of mononucleosomal DNA fragments and poly(styrenesulfonic acid) with tetramethylammonium (TMA^+) counterions.[11–14] It was seen that by optimizing some of the geometric parameters, the classical PB or modified Poisson–Boltzmann (MPB) theory gives a good description of the structure.[15–17] In the present contribution these investigations are extended to DNA fragments (157 base pair) with multivalent polyamine counterions.

We have used the linear polyamines putrescine (Pu^{2+}):

$$H_3N^+–CH_2–CH_2–CH_2–CH_2–N^+H_3$$

and spermidine (Sp^{3+})

$$H_3N^+–CH_2–CH_2–CH_2–CH_2–N^+H_2–CH_2–CH_2–CH_2–N^+H_3.$$

Note that the polyamines are in the protonated charged state, with the charges localized at the nitrogen positions. Putrescine is soluble at all ligand/DNA ratios, whereas spermidine induces condensation if its charge fraction exceeds a certain critical fraction of the total DNA charge. Simple salt free $Pu–DNA_2$ was prepared by exchanging the monovalent counterions for Pu^{2+}. This counterion exchange procedure is not possible with spermidine and, instead, we have prepared Na–DNA solutions with added $SpCl_3$ salt in 5:1 molar ratio. In the latter solutions, the sodium and chloride ions do not contribute to the scattering to any significant degree because of negligible scattering length contrast. Accordingly, for both $Pu–DNA_2$ and $Na–DNA/SpCl_3$ solutions, the scattered intensities are sensitive to correlations among the DNA and polyamine densities only.

For DNA, the linear charge density is so high that most counterions are confined to the immediate vicinity of the polyion and concentration fluctuations are expected to have little impact on the radial counterion densities. The central hypothesis in our experimental approach is the neglect of influence on the double layer structure due to fluctuations in inter-DNA separation and orientation. With this hypothesis, the DNA–DNA, polyamine–polyamine, and DNA–polyamine partial structure factors should satisfy certain conditions.[14] Explicit use of these conditions in the data analysis procedure results in improved statistical accuracy in the structure factors. It will be shown in this work that this conjecture holds and that information on the counterion distribution can be obtained without considering the interactions between double layers pertaining to different DNA fragments. The effect of polyamines on the DNA molecular structure is gauged from a comparison of the DNA structure factor with the high q limiting form of the form function of a rod with a finite cross-sectional radius of gyration. The double layer structure and the extent to which the polyamines can approach the DNA are derived from the DNA–counterion and counterion–counterion partial structure factors. For this purpose, the latter structure factors are interpreted with the radial counterion profiles obtained from the PB, MPB equations, and/or Monte Carlo (MC) simulation.[18–20] Earlier works indicate that for multivalent counterions ionic correlation effects on the double layer formation are significant.[19,20] Finally, for simple salt free DNA, spatial fluctuations in the charge density are discussed in terms of the charge structure factor.

II. THEORY

A. Scattering

For a three component system, the coherent part of the solvent corrected SANS intensity reads

$$I(q)/\rho_L = \overline{b_m^2} N_m^2 S_{mm}(q) + 2\,\overline{b_m}\,\overline{b_c} N_m N_c S_{mc}(q) + \overline{b_c^2} N_c^2 S_{cc}(q) \tag{1}$$

with ρ_L the DNA concentration. The number of nucleotide monomer (m) and counterions (c) per DNA fragment are denoted by N_m and N_c with macroscopic concentrations $\rho_m = N_m \rho_L$ and $\rho_c = N_c \rho_L$, respectively. In the absence of inter-DNA interactions, the partial structure factors S_{ij} are normalized to unity at $q=0$.[21] In an H_2O/D_2O solvent mixture, the scattering length contrast is given by

$$\overline{b_i} = b_i - b_s \overline{v_i}/\overline{v_s}; \quad b_s = X\, b_{D_2O} + (1-X)\, b_{H_2O} \tag{2}$$

with X the D_2O mole fraction. The solute ($i=m,c$) and solvent (s) have scattering lengths b_i and b_s and partial molar volumes $\overline{v_i}$ and $\overline{v_s}$, respectively. The partial structure factors S_{ij} are the spatial Fourier transforms of the solute density correlation functions[6]

$$S_{ij}(q) = \frac{1}{\rho_L N_i N_j} \int_V d\vec{r} \exp(\vec{q}\cdot\vec{r}) \langle \rho_i(0) \rho_j(\vec{r}) \rangle. \tag{3}$$

In our experiments, the partial structure factors are obtained from the intensities by contrast variation in water, i.e., by adjusting the solvent scattering length b_s. The partial structure factors can be further evaluated theoretically from the density correlation functions derived from the cell model.

B. Cell model

For cylindrical polyelectrolytes, a self-consistent charge distribution can be obtained using the cell model and the solution of the PB, MPB equations, and/or MC simulations.[15,16,18–20] The requirement for applying the cell model is that the DNA chain is *locally* rodlike over a length far exceeding the double layer thickness and bearing a sufficiently large number of charges. The fragment is assumed a uniformly charged rod with length L and is placed along the z axis of a coaxial cylinder of the same length L and radius r_{cell}. The cell radius is determined by the nucleotide concentration ρ_m through $\rho_m A \pi r_{cell}^2 = 1$, with the longitudinal axis projected nucleotide repeat distance $A = 0.171$ nm. In the longitudinal direction (along the DNA axis), the nucleotide and counterion distributions are assumed uniform while per-

pendicular to this axis, the corresponding densities are given by the *radial* concentration profiles $\rho_m(r)$ and $\rho_c(r)$, respectively.

Within the present range of momentum transfer ($qL \gg 1$) the scattering is sensitive to correlations over distances of the order of the double layer thickness and the effects of finite contour length and flexibility are negligible. In the cell model the effects of fluctuations in inter-DNA separation and orientation (i.e., DNA density fluctuations and hence fluctuations in cell radius) on the double layer structure are neglected. It is shown in the Appendix that with this assumption the partial structure factors can be expressed as a product of terms involving the radial profiles and a term related to the polymer structure[14]

$$S_{ij}(q) = S(q) a_i(q)\, a_j(q) \quad (qL \gg 1) \tag{4}$$

with the cylindrical Fourier (Hankel) transformation of the radial profile

$$a_i(q) = 2\pi \int_0^{r_{\text{cell}}} dr\, r J_0(qr) \rho_i(r) \quad (i = m, c) \tag{5}$$

and J_0 denotes the zero order Bessel function of the first kind. The polymer term S describes the (inter- and intramolecular) structure of an equivalent solution, but for rods with vanishing cross-section [see Eq. (A5)]. For sufficiently high values of momentum transfer and/or low DNA concentration, inter-DNA correlations are insignificant and S reduces to the form function of a rigid rod. Accordingly, the high q limiting form of the single-cell partial structure factor takes the form

$$S_{ij}(q) \approx \frac{\pi}{qL} a_i(q) a_j(q) \quad (qL \gg 1). \tag{6}$$

For lower values of momentum transfer and/or higher DNA density, correlations between different cell volumes become progressively more important and the experimental data deviate from the single cell calculations. However, the polymer term S (and, hence, inter-DNA interference) can be eliminated by taking the ratio of the nucleotide–counterion S_{mc} and nucleotide monomer S_{mm} structure factor:

$$\frac{S_{mc}(q)}{S_{mm}(q)} = \frac{a_c(q)}{a_m(q)} \quad (qL \gg 1). \tag{7}$$

From the full set of partial structure factors information on the radial counterion density profile can be obtained, without a model of interchain correlations. Furthermore, for $qL \gg 1$ the scattering is dominated by configurations in which the momentum transfer is oriented perpendicular to the DNA molecule ($\mu = 0$, see the Appendix) and, hence, any charge ordering along the DNA is difficult to detect.

In the derivation of Eq. (4) small ion density fluctuations are neglected. These fluctuations give an additional scattering contribution to the counterion structure factor S_{cc} only. The cross term S_{mc} [and, hence, the ratio in Eq. (7)] is unaffected due to the heterodyne interference between the amplitudes scattered by the DNA and the counterions. For highly charged polyelectrolytes, the additional scattering contribution has not been evaluated yet, but it is expected to be modest in comparison with the pronounced contribution due to the average profile.

TABLE I. Geometric parameters 157 base pair DNA in nm. A, spine-axis projected repeat distance; r_p, cross-sectional DNA radius of gyration; r_{ci}, counterion radius; r_c, distance of closest approach to the DNA spine axis; r_{cell}, cell radius (0.05 mole nucleotides/dm^3); L_p, persistence length; L, contour length.

		r_{ci}			r_c					
A	r_p	TMA^+	Pu^{2+}	Sp^{3+}	TMA^+	Pu^{2+}	Sp^{3+}	r_{cell}	L_p	L
0.171	0.8	0.40	0.30	0.35	1.45	1.35	1.40	*7.9*	50	54

C. Radial profiles

The transform Eq. (5) can be further evaluated using analytical expressions of the radial densities. If the radial DNA density is assumed to be uniform for $0 \leqslant r \leqslant r_p$ and given by $\rho_m(r)\pi r_p^2 = 1$ and zero for $r > r_p$, with r_p the DNA radius, one obtains

$$a_m(q) = \frac{2J_1(qr_p)}{qr_p} \tag{8}$$

with J_1 the first order Bessel function of the first kind. The DNA cross section might also be described by a Gaussian radial density profile with second moment $\langle r^2 \rangle = r_p^2/2$. In the present range of momentum transfer, the Hankel transform of such Gaussian profile is very similar to Eq. (8) and the radius r_p can be interpreted as a cross-sectional radius of gyration of the DNA molecule.

The radial counterion density profile $\rho_c(r)$ is obtained from the solution of the PB and MPB equations, and the MC simulations in the cylindrical cell model.[15,16,18–20] Apart from the cell radius, the structural parameters are the counterion radius, the distance of closest approach between the counterion center of mass and the DNA spine-axis r_c, and the linear charge density parameter $\xi = Q/A$, Q being the Bjerrum length [$Q = e^2/(4\pi\varepsilon_0\varepsilon_r k_B T)$]. In the classical PB equation, the counterions are treated as pointlike particles and the effect of counterion radius is taken into account through the distance of closest approach. In the MPB and MC treatments, which include ionic correlation effects, the counterions are modeled as hard sphere ions (despite the fact that polyamines are linear molecules). The distance of the closest approach is not necessarily equal to the DNA radius r_p; rather, one expects a slightly larger value due to counterion size and intermediate hydration shell.

The classical PB equation for salt free solutions for a single species of counterions in the cell is solvable analytically,[15,16] while more general cases with several species of simple ions require numerical solution for the dimensionless potential $\phi(r)$. We used fourth- and fifth-order Runge–Kutta formulas, and the counter- and co-ion concentrations at the cell boundary were optimized to satisfy the boundary conditions $\phi(r_{\text{cell}}) = 0$ and $\phi'(r_c) = 2\xi/r_c$, where the prime denotes differentiation with respect to the radial coordinate r.[22] The distance of closest approach, cell radius, and nucleotide (charge) repeat distance were fixed at their

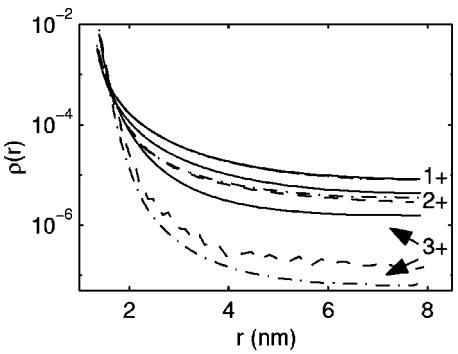

FIG. 1. Counterion concentration profile versus distance away from the DNA axis. Solid, dashed–dotted, and dashed curves refer to PB, MPB, and MC calculations, respectively. The profiles are calculated with the parameters in Table I.

nominal values listed in Table I. For simple salt free solutions, the numerical results agree with the analytical solution for a single species counterion in the cell.[15,16]

The MPB approach attempts to improve upon the PB treatment by incorporating the ionic correlation and exclusion volume effects. Details of the MPB equation for the cell model in cylindrical geometry have been described in Refs. 17, 19, and 20. Numerical solution of the MPB equation was obtained through a quasi-linearization iterative technique. The same method applied to the PB equation gave identical results to that from the Runge–Kutta technique, which, in turn, coincided with the analytic solution in the case of salt free solutions with one species of counterions only.[15,16] This served as a useful check on some of the numerics.

The MC simulations involved standard canonical metropolis algorithm. Again essentially the same procedure as described in Refs. 19 and 20 was adopted. In most cases, the length of the central simulation box corresponded to a polyion segment with $2\times10^2-4\times10^2$ monomer units. In a typical run around $8\times10^6-10\times10^6$ configurations were sampled of which $2\times10^6-3\times10^6$ configurations were used for equilibration.

The radial counterion profiles obtained from PB, MPB, and MC calculations are displayed in Fig. 1. With increasing valence, the counterion concentration close to the DNA surface increases with a concurrent decrease for larger distances. For monovalent counterions, the three theoretical approaches give similar results, showing that the inclusion of ionic correlation effects does not change the profile to a significant degree. In the case of divalent and especially for trivalent counterions however, the more elaborate MPB and MC results are close together and show a stronger confinement in comparison with the classical PB approach. These results reinforce similar conclusions reached in earlier works.[19,20]

III. EXPERIMENTAL SECTION

A. Solutions

DNA fragments were obtained by micrococcal nuclease digestion of calf thymus chromatin.[23] After precipitation in cold 2-propanol, the DNA pellet was dried under reduced pressure at room temperature. The DNA was brought to the salt free sodium form by dissolving it in a 50 mM NaCl, 24 mM EDTA buffer and extensive dialysis against water (purified by a Millipore system with conductivity less than $1\times10^{-6}\,\Omega^{-1}\,\mathrm{cm}^{-1}$). To avoid denaturation, care was taken that the DNA concentration did not drop below 3×10^{-3} mole of nucleotides/dm^3. The differential molecular weight distribution was monitored by size exclusion chromatography (SEC) with light scattering detection.[24] Further SEC fractionation resulted in a relatively monodisperse mononucleosomal DNA eluent fraction with weight average molecular weight $M_w=104\,000$ (157 base pairs) and $M_w/M_n=1.14$. The ratios of the optical absorbencies $A_{260}/A_{280}=1.91$ and $A_{269}/A_{270}=1.21$ indicate that the material is essentially free of protein and phenol, respectively.[25] DNA with Pu^{2+} counterions was prepared by pouring a Na–DNA solution through a cation exchange resin (Biorad AG 50W X8). Atomic absorbance spectroscopy showed that the residual sodium content in Pu–DNA_2 (without salt) is less than 1%. The hypochromic effect at 260 nm exceeds 35%, which confirms the integrity of the double helix.

TABLE II. Concentrations in mole/dm^3. (–) Not present or less than 1%.

Set	Solute	DNA	Na^+	Pu^{2+}	Sp^{3+}	Cl^-
I	Pu–DNA_2	0.10	–	0.05	–	–
II	Pu–DNA_2	0.05	–	0.025	–	–
III	Na–DNA/$SpCl_3$	0.10	0.10	–	0.02	0.06
IV	Na–DNA/$SpCl_3$	0.05	0.05	–	0.01	0.03

Concentrations were determined by weight, using the water content in the freeze-dried materials, and checked with UV spectroscopy. Four sets of samples were prepared. The first two sets were made with 0.1 and 0.05 mole nucleotide/dm^3 Pu–DNA_2, respectively (i.e., without added simple salt). The second two sets contain mixtures of Na–DNA and $SpCl_3$ with nucleotide concentrations 0.1 and 0.05 M, respectively. In the latter two sets, the molar ratio between Na–DNA and $SpCl_3$ is fixed at 5 to 1. The ion concentrations are listed in Table II. For contrast variation, each set was prepared in 0, 33, 63, and 99 % D_2O. The solvent compositions were determined by weight and checked with IR spectroscopy. Scattering length contrasts were calculated with Eq. (2) and the parameters in Table III and are collected in Table IV. The DNA scattering length has been calculated using the values reported by Jacrot[26] and according to the calf thymus base composition A:G:C:T:5-methylcytosine $=0.28:0.22:0.21:0.28:0.01$. Reference solvent samples with matching H_2O/D_2O composition were also prepared. Stan-

TABLE III. Partial molar volumes and scattering lengths. X denotes the D_2O mole fraction (effect of exchangeable hydrogen).

Solute	$\bar{v}_i$ (cm^3/mole)	b_i (10^{-12} cm)
DNA	172	9.772+2.020X
Sp^{3+}	140	−0.765+8.328X
Pu^{2+}	95	−0.704+6.246X
H_2O	18	−0.168
D_2O	18	1.915

TABLE IV. Scattering length contrast in 10^{-12} cm.

Solvent	$\bar{b}_{DNA}$	$\bar{b}_{Pu}$	$\bar{b}_{Sp}$
H_2O	11.4	0.3	0.5
33% D_2O	5.5	−1.4	−2.0
63% D_2O	0.1	−2.8	−4.4
99% D_2O	−6.3	−4.5	−7.2

dard quartz sample containers with 0.1 cm (for samples in pure H_2O) or 0.2 cm path length were used.

B. Scattering

SANS experiments were done with the D11 and D22 diffractometers, situated on the cold source of the high neutron flux reactor at the Institute Max von Laue–Paul Langevin (ILL), Grenoble, France. The temperature was kept at 293 K. Sample sets I and III (see Table II) were measured with the D22 instrument in two different configurations. A wavelength of 0.7 nm was selected and the effective distances between the sample and the planar square multidetector (S–D distance) were 1.25 and 4 m, respectively. This allows for a momentum transfer range of 0.1–4.1 nm^{-1}. Sets II, III (duplicate measurement), and IV were collected with the D11 instrument in two different configurations. The wavelength was fixed at 0.5 nm and the detector was subsequently placed at 4 and 8 m from the sample position. These S–D distances allow for a momentum transfer range of 0.2–3.6 nm^{-1}. The counting times were approximately 2 h/sample, irrespective instrument and S–D distance. Data correction allowed for sample transmission and detector efficiency. The efficiency of the detector was taken into account with the scattering of H_2O. Absolute intensities were obtained by reference to the attenuated direct beam and the scattering of the pure solvent with the same H_2O/D_2O composition was subtracted. Finally, the intensities were corrected for a small solute incoherent scattering contribution. From the duplicate measurements of sample set III, it was checked that the data collected with both instruments match.

The scattered intensities display an upturn at very low q values ($q<0.2$ nm^{-1}). This upturn is more or less proportional to the D_2O mole fraction and becomes very small (or disappears completely) in H_2O. Similar behavior has been observed in synthetic poly(styrenesulfonic acid) solutions, despite completely different contrast parameters.[12] Accordingly, the upturn is induced and/or amplified by the use of D_2O and is not related to a solvent composition independent inhomogeneity in solution structure. The difference in the dielectric constants of light and heavy water is very small [$\varepsilon_r=80.4$ and 79.8, respectively, at 293 K] and concomitant effects on the charge distribution are insignificant. A number of experimental parameters have been checked, such as D_2O purity, cell path length, pulsed and reactor neutron sources, and different diffractometers, but a satisfactory explanation has not been offered.[11,12,14] For higher q values, the intensities comply with solvent composition independent structure factors. Accordingly, it is assumed that for $q>0.2$ nm^{-1} the data are not influenced by this effect. For $q>3$ nm^{-1} the intensities become very small of the order of the error margin 5×10^{-3} cm^{-1}.

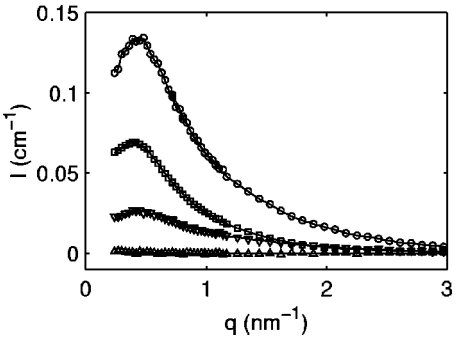

FIG. 2. Experimental SANS intensity versus momentum transfer from 0.05 mole of nucleotides/dm^3 Pu–DNA_2. The H_2O/D_2O solvent composition is 0, 100, 33, and 63 % D_2O from top to bottom. The lines represent a two-parameter fit in which the partial structure factors are optimized.

IV. RESULTS AND DISCUSSION

A. Data analysis

For simple salt free solutions, all ions come from the DNA and there are three molecular components only: solvent, DNA nucleotide monomers, and counterions. The solvent is treated as a uniform background and a description of the structure thus requires three partial structure factors. In the case of Na–DNA solutions with added $SpCl_3$, the salt gives two additional components and, now, the structure is given by 10 partial structure factors. The Cl^- and Na^+ ions do not contribute to the scattering to any significant degree, due to negligible scattering length contrast. Accordingly, for an analysis of scattering data, the Na–DNA/$SpCl_3$ solutions can be considered as three component systems as well. The counterions, which contribute to the scattering, are derived either from the DNA (Pu^{2+} in salt free solutions) or from the salt (Sp^{3+} in Na–DNA with added $SpCl_3$).

The DNA–DNA, DNA–counterion, and counterion–counterion partial structure factors can be obtained from the scattered intensities of samples with different contrast length parameters. As an example, Fig. 2 displays the intensities of 0.05 M Pu–DNA_2 with contrast matching in the water. The other samples show similar behavior, except for the suppression of the correlation peak in the low q region in the presence of $SpCl_3$ (data not shown). Note that in 63% D_2O solution DNA is blanked, and the scattering is directly proportional to the counterion structure factor. With four experimental intensities and three unknown partial structure factors per set, the data is overdetermined and the partial structure factors can be derived by orthogonal factorization in a least-squares sense (i.e., a three-parameter fit to four data points for every q value). For 0.05 M Pu–DNA_2, the results are shown by the symbols in Fig. 3. The statistical accuracy of the counterion–counterion structure factor is especially poor, due to the moderate Pu^{2+} scattering length contrast (Table IV) and relatively low solute concentrations.

The accuracy of the derived partial structure factors can be improved with the assumption that the double layer struc-

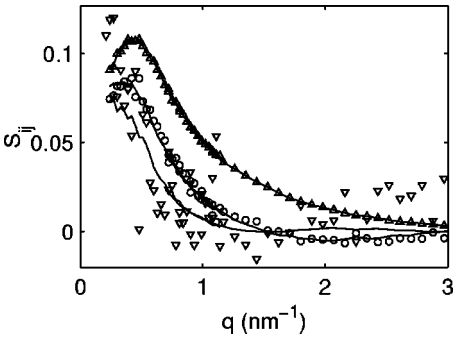

FIG. 3. DNA–DNA (△), DNA–Pu^{2+} (○), and Pu^{2+}–Pu^{2+} (▽) partial structure factors in 0.05 mole of nucleotides/dm^3 Pu–DNA_2 solutions obtained from a three-parameter fit. The solid curves result from a two-parameter fit.

ture is invariant to DNA concentration fluctuations. In this case, the partial structure factors can be expressed as a product of terms involving the radial profiles and a term describing the polymer structure, but for rods with vanishing cross section [Eq. (4)]. In previous work, it was shown that for DNA with TMA^+ counterions the structure factors (obtained from a three-parameter fit) indeed satisfy Eq. (4).[14] The polymer structure term $S(q)$ is positive definite, due to the fact that it represents a scattered intensity (i.e., squared amplitude). Accordingly, with Eq. (4) the intensities Eq. (1) can be expressed in terms of two unknown factors $u_i(q) = S(q)^{1/2} a_i(q)$ rather than three partial structure factors $S_{ij}(q)$ $(i,j=m,c)$. With a nonlinear least-squares procedure, the two factors $u_i(q)$ were fitted to the data and the partial structure factors were reconstructed according to Eq. (4). The fitted intensities and the derived partial structure factors are given by the solid curves in Figs. 2 and 3, respectively. Now, the statistical accuracy has improved and the partial structure factors agree with the results obtained from the model-free three-parameter fit. This agreement is particularly gratifying in the case of the cross term, which describes the density correlations between the DNA and the counterions and, hence, gives the double layer structure.

All of the data was analyzed with the two-parameter procedure and similar agreement was observed (data not shown). The DNA–DNA partial structure factor multiplied by momentum transfer is displayed in Fig. 4. The DNA–counterion and the counterion–counterion partial structure factors are shown in Figs. 5 and 6, respectively. In the latter two figures, we have also included previously reported results pertaining to salt-free DNA with monovalent TMA^+ counterions (but reanalyzed with the two-parameter procedure).[11,13] For the sake of comparison, all structure factors are normalized to unity in the $q \to 0$ limit and in the absence of inter-DNA correlations.[21] Due to the accumulation of counterions around DNA, the DNA–counterion partial structure factor shows a minimum corresponding to a *negative* value of the structure factor at $q \approx 2$ nm^{-1}. For the same reason, the counterion–counterion partial structure factor displays a singularity and secondary maximum at $q \approx 1.5$ and 2 nm^{-1}, respectively. The positions of these features are very sensitive to the distance of closest approach between the counterion and the DNA (see below).

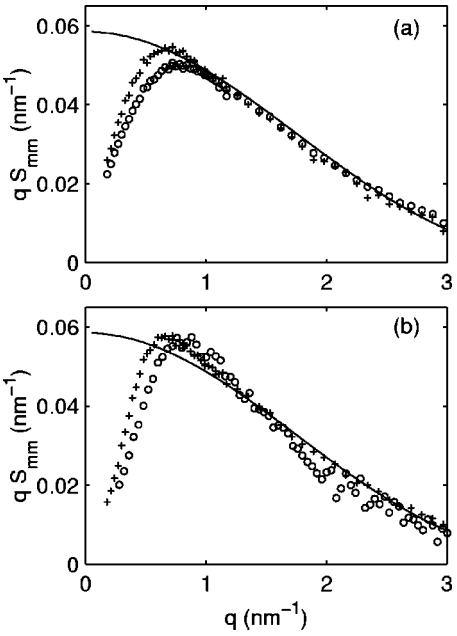

FIG. 4. DNA structure factor multiplied by momentum transfer: (a), Na–DNA/$SpCl_3$; (b), Pu–DNA_2. The nucleotide concentrations are 0.05 (+) and 0.1 (○) M. The solid lines denote the high q limiting form of the rigid rod form function times q, with $r_p = 0.8$ nm and $L = 54$ nm ($A = 0.171$ nm).

B. DNA structure

For Pu–DNA_2 and Na–DNA with added $SpCl_3$, no high q plateau value in the qS_{mm} versus q plot is observed in Fig. 4. The finite DNA cross section is responsible for the absence of rodlike q^{-1} scaling, as has previously been observed in Na–DNA fragment solutions with excess KBr.[27] For q exceeding, say, 1 nm^{-1}, the structure factors approach the limiting form of the rigid rod form function Eq. (6), $(i,j=m)$ with the Hankel transform Eq. (8) of a steplike nucleotide profile. The fragments have weight average contour length $L = 54$ nm and, hence, flexibility effects on the form function are less than 4% for the lower bound $qL \approx 5$ and become negligible as q is increased.[28] The optimized value of the DNA radius r_p is 0.8 nm. A Gaussian radial profile gives an equally good fit (results not shown) and r_p can be considered a cross-sectional radius of gyration. The value of r_p agrees with the previously reported value for DNA with monovalent alkali counterions and is slightly smaller than the outer radius of 1 nm for a double helix in the B form.[27] This difference can be rationalized on the basis of the relatively open molecular structure and the existence of grooves. Multivalent polyamines have no detectable effect on the DNA cross-section and the z-axis-projected distance between nucleotides (0.171 nm).

In the low q region, the data deviate from the intrachain function due to inter-DNA correlations. For the salt free Pu–DNA_2, a correlation peak at finite wavelengths is observed, which shifts to lower q values with decreasing DNA concentration according to $\rho_L^{1/2}$. The peak position and its concentration scaling are similar to those reported for DNA fragment solutions with monovalent counterions.[27] In the case of Na–DNA with added $SpCl_3$, the correlation peak is

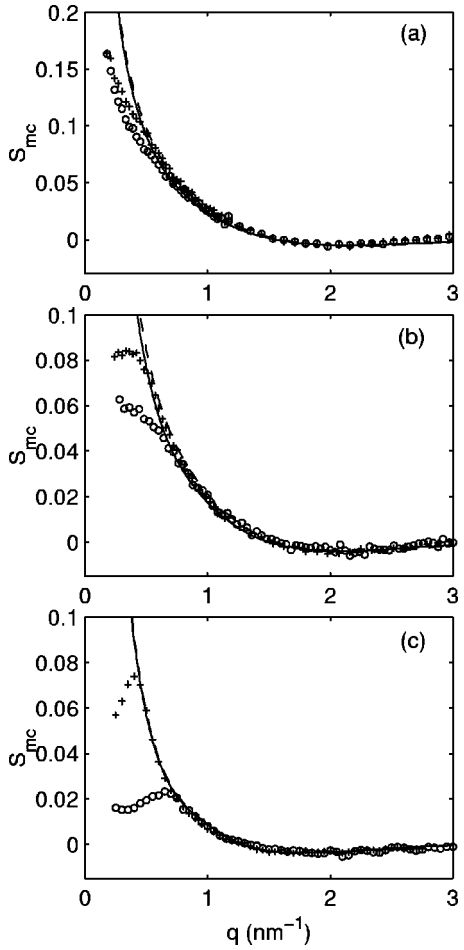

FIG. 5. DNA–Sp^{3+} (a), DNA–Pu^{2+} (b), and DNA–TMA^{+} (c) cross partial structure factor versus momentum transfer. The nucleotide concentrations are 0.05 (+) and 0.1 (○) M. The curves represent the single cell expression Eq. (6) with radial counterion profiles from PB (solid lines) and MC (dashed lines) calculations.

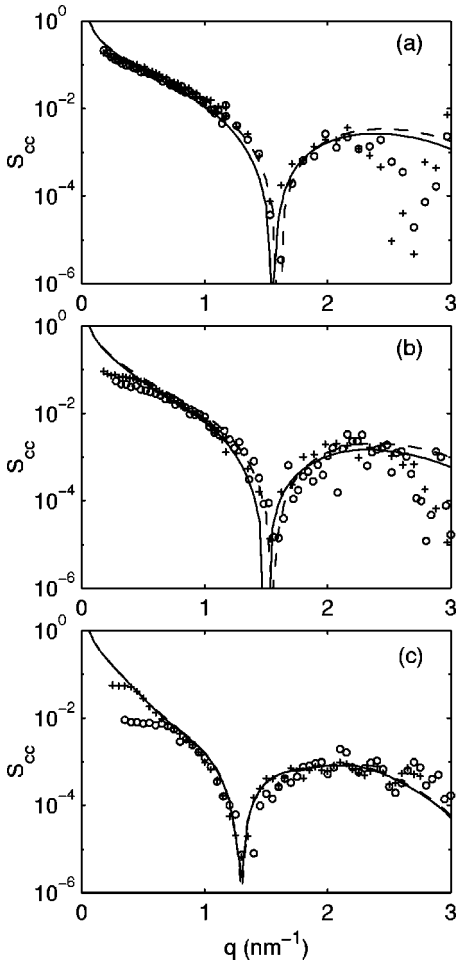

FIG. 6. As in Fig. 5, but for the Sp^{3+} (a), Pu^{2+} (b), and TMA^{+} (c) counterion partial structure factor.

suppressed with a concurrent increase in intensity in the smaller q region. However, a complete discussion of the inter-DNA solution structure is beyond the scope of the present contribution (see Ref. 27 for a discussion of the DNA fragment solution structure in the presence of monovalent salt). Here, we will focus on the double layer structure, which is reflected in a direct manner by the DNA–counterion and counterion–counterion partial structure factors.

C. Double layer structure

The normalized DNA–counterion and counterion–counterion partial structure factors for mono-, di-, and trivalent (TMA^{+}, Pu^{2+}, and Sp^{3+}) counterions are displayed in Figs. 5 and 6, respectively. With increasing counterion valence the double layer becomes more confined and, hence, both structure factors scale toward higher values of momentum transfer. As in the case of the DNA–DNA structure factor, the counterion involved partial structure factors exhibit a peak (for Pu–DNA_2) or suppression in the low q region (with excess $SpCl_3$) due to interference effects between double layers pertaining to different DNA molecules. For higher values of momentum transfer, these interference effects become progressively less important and the structure factors reflect the counterion organization around a single DNA molecule. Accordingly, in the corresponding q region the (normalized) structure factors obtained for the different nucleotide concentrations superpose and may be compared with the single-cell calculations.

The single-cell partial structure factors were calculated with the high q limiting form Eq. (6) and the radial counterion profiles based on the classical PB and MPB equations, and/or MC simulation (see Fig. 1). With our lower bound $qL \approx 5$ finite DNA contour length and flexibility effects on the structure factors are insignificant. The results are denoted by the curves displayed in Figs. 5 and 6 and refer to 0.05 mole of nucleotides/dm^3. For 0.1 M DNA the theoretical predictions are similar (not shown). The MPB results are very close to the MC simulation results and are not displayed for reasons of clarity. In the MC simulation, the distance of closest approach r_c was optimized in order to reproduce the positions of the minimum in the counterion structure factors (Table I). Nice agreement is observed in the high q region where interference effects between different cell volumes become progressively less important. In particular, the scaling of the structure factors toward higher values of momentum transfer with increasing counterion valence is reproduced. The MC, MPB, and PB results are close, or even superpose

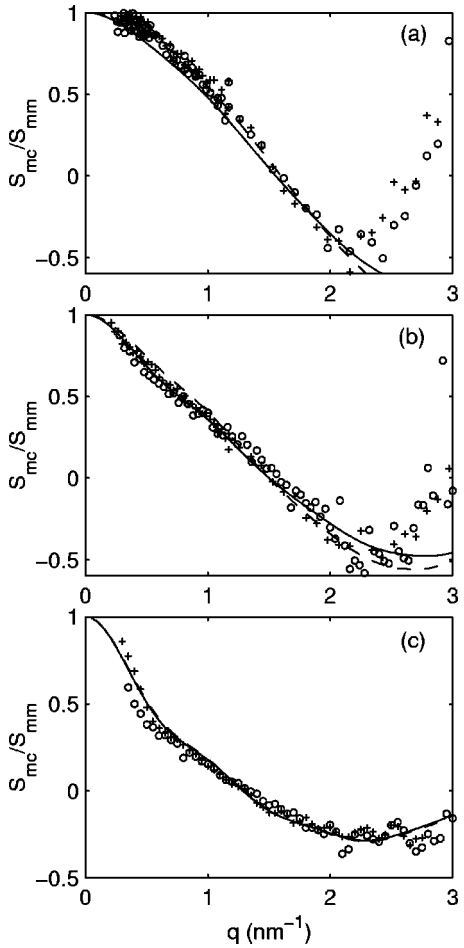

FIG. 7. As in Fig. 5, but for the ratio of the DNA–counterion and DNA (nucleotide) partial structure factors.

in the case of monovalent counterions, and, from these results, it is hard to prefer one theoretical approach to another. Such behavior of monovalent counterions is of course well known in the double layer literature.

For lower values of the momentum transfer, the data deviate from the single-cell predictions and a complete analysis of the DNA interactions seems to be necessary. However, if the assumptions leading to Eq. (4) hold, low q interference effects can be eliminated in taking the ratio Eq. (7) of the DNA–counterion and DNA–DNA structure factor. Indeed, as observed in Fig. 7, inter-DNA correlations are effectively cancelled and the data pertaining to two different nucleotide concentrations (0.05 and 0.1 M) coincide. Now, the comparison with the theoretical cell-model predictions can be extended to the low q region. In the case of Pu–DNA_2, the PB prediction seems to be in better agreement with the data, but the difference with the MC or MPB results is of the order of the experimental reproducibility. In the case of trivalent Sp^{3+}, the classical PB equation clearly underestimates the counterion confinement and the MC simulation or MPB approach is superior in predicting the structure factor. Especially for the polyamines in the higher q range ($q > 2.5$ nm^{-1}), the data deviate from the theoretical predictions. This can be attributed to the neglect of the internal counterion molecular structure in the calculation of the structure factors.

The distance of closest approach r_c between the counterion center of mass and the DNA spine-axis agrees with the physical extent of the DNA molecule (with cross-sectional radius of gyration $r_p = 0.8$ nm), hydration shell, and counterion size. For instance, in TMACl solutions with cation concentrations similar to those within the double layer, intermolecular correlations about TMA^+ start rising at ~ 0.36 nm and peak at ~ 0.46 nm from the central nitrogen atom.[29] If the TMA^+ counterion is drawn into close contact with the DNA phosphates with a concurrent displacement of hydration water, r_c is expected to take a value around 1.45 nm. Of course, the polyamines are linear molecules, whereas in the calculations they have been modeled as charged hard spheres. The low resolution of the SANS experiment and the fact that the structure factors are averaged over DNA orientation do not warrant a more detailed description of the molecular structure. Accordingly, the distances of closest approach in Table I should be interpreted as averaged values over polyamine orientation and different DNA sites; e.g., polyamines near the grooves might be arranged differently than those near the phosphates.[5] For the polyamines, the optimized distances of closest approach are comparable to the TMA^+ value, which shows that the polyamines also do not significantly penetrate the grooves nor come very close to the DNA surface.

D. Charge ordering

For simple salt free solutions, every charge carrier is associated with a DNA nucleotide or counterion. Accordingly, for the latter systems it is of interest to construct the charge–charge structure factor[30]

$$S_{zz}(q) = S_{mm}(q) - 2S_{mc}(q) + S_{cc}(q) \tag{9}$$

which describes the spatial fluctuations in charge density and is particularly sensitive to the ordering of the ions.[31] This factor displays a characteristic maximum at wavelengths of the order of the inverse double layer thickness. The charge structure factor should obey the Stillinger–Lovett sum rules.[32] In the $q \to 0$ limit the charge structure goes to zero because of overall charge neutrality. By expanding Eq. (9) up to the second power of q, one obtains the second moment of the charge density pair correlation, which is a definition of the screening length. For high q values, the charge structure factor decreases with increasing q, because the internal structure of the charge carriers is probed. With Eq. (4) the cell model expression of the charge structure factor reads

$$S_{zz}(q) = S(q)\,(a_m(q) - a_c(q))^2 \quad (qL \gg 1) \tag{10}$$

with the single-cell high q limiting form

$$S_{zz}(q) = \frac{\pi}{qL}(a_m(q) - a_c(q))^2 \quad (qL \gg 1). \tag{11}$$

The first term of the expansion of the radial terms is proportional to q^4, whereas correlations between different cell volumes can be made arbitrarily small at high polyion dilution. Accordingly, it is necessary to include counterion fluctuations about the average profile if we wish to satisfy the sec-

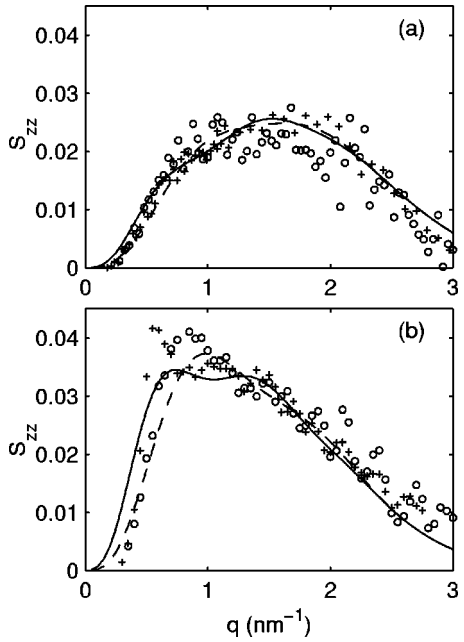

FIG. 8. Charge structure factor for simple salt free Pu–DNA_2 (a) and TMA–DNA (b). The nucleotide concentrations are 0.05 (+) and 0.1 (○) M. The curves represent the limiting form of the single cell expression Eq. (11) with radial counterion profiles from the classical PB calculation (solid and dashed lines for 0.05 and 0.1 M solutions, respectively).

ond moment sum rule.[33] Furthermore, the charge structure factor is related to the static longitudinal dielectric function $\varepsilon(q)$, which is a q-dependent generalization of the macroscopic dielectric constant.[3]

For salt free TMA–DNA and Pu–DNA_2 solutions, the charge structure factor is displayed in Fig. 8. The data approach zero in the long wavelength limit and show a maximum at finite values of momentum transfer. With increasing counterion valence, the maximum decreases and its position shifts to higher q values. This is related to the stronger charge confinement and the decrease in range over which the charges are allowed to fluctuate with increasing Coulomb coupling. The effect of DNA concentration is most clear in the case of TMA–DNA. Here, the charge structure factor shifts to lower values of momentum transfer and becomes oscillatory with decreasing concentration. With an increase in available volume, the screening decreases with a concurrent increase in charge ordering. The latter phenomenon occurs because the counterion concentration far away from the DNA can now drop to lower values. For the more diluted 0.05 M Pu–DNA, this oscillatory behavior is also observed, although less pronounced due to the stronger Coulomb interaction.

The single-cell calculation Eq. (11) with the radial counterion profile based on the classical PB equation is also displayed in Fig. 8. Double layer theory predicts the ordering and the range over which the charges are allowed to fluctuate satisfactorily. Features such as the effect of counterion valence, DNA concentration, and the onset of oscillatory behavior are nicely reproduced. In particular for TMA–DNA, in the low q region deviations from the single-cell calculation are observed due to interference between double layers pertaining to different DNA molecules. Despite this interference effect, the data are close to the single-cell calculation and do not show a limiting q^2 behavior. With the profiles resulting from MC simulation, the theoretical predictions are similar (TMA^+) or a little different within experimental reproducibility (Pu^{2+}).

V. CONCLUSIONS

With a view to describing the structural arrangement of condensing ligands near DNA, we have obtained the DNA–DNA, polyamine–polyamine, and DNA–polyamine partial structure factors. From the high q behavior of the DNA–DNA structure factor, it was observed that multivalent counterions have no detectable effect on the DNA local structure, i.e., the cross-sectional radius of gyration and the distance between nucleotides. The partial structure factors that involve the counterions are sensitive to the distance of closest approach of the counterion center of mass to the DNA spine axis. The optimized values for Pu^{2+} and Sp^{3+} are similar to the value for TMA^+ and agree with the physical extent of the DNA molecule, hydration water, and counterion size. This shows that the polyamines do not significantly penetrate the grooves and/or come very close to the DNA surface. Any spatial inhomogeneity in dielectric permittivity close to DNA results in a scaling of the structure factors towards higher values of momentum transfer (due to stronger counterion confinement) and, hence, cannot compensate for the effect of a smaller distance of closest approach.[34]

All the structure factors are sensitive to interference between double layers pertaining to different DNA molecules. In taking the ratio of the DNA–polyamine and the DNA–DNA structure factors, these interference effects are effectively cancelled and data collected from solutions with different nucleic acid concentrations superpose. This observation strongly supports our hypothesis concerning the neglect of correlation between fluctuations in inter-DNA separation and orientation and double layer structure. With increasing counterion valence, the ratio of the structure factors scales toward higher values of momentum transfer, in agreement with a stronger confinement due to increased Coulomb coupling. The data can be interpreted with radial counterion profiles derived from the PB and MPB theories or the MC simulation within a single-cell volume. For monovalent counterions, the various theoretical approaches yield similar results. In the case of Pu–DNA_2, the PB prediction seems to be in better agreement, but the difference with the MPB or MC results is of the order of the experimental reproducibility. For trivalent Sp^{3+}, ionic correlation effects are most pronounced and the MPB theory (or MC simulation) is superior in predicting the structure factors.

For simple salt free TMA–DNA and Pu–DNA_2 solutions, the charge structure factor is derived and interpreted with the single-cell predictions. The theory predicts the charge ordering and the range over which the charges are allowed to fluctuate satisfactorily. Features such as the effects of counterion valence and DNA concentration are nicely reproduced. With decreasing concentration the onset of oscillatory behavior is observed, which should reflect in the q dependent generalization of the dielectric constant. The

data do not show a limiting q^2 behavior, which indicates that the contribution given by counterion fluctuations is small.

The structural arrangement of Pu^{2+} and Sp^{3+} can be fully rationalized in terms of their valence; the distances of closest approach are similar and comparable to the value for TMA^+. These ions are too large to penetrate the grooves to any significant extent. In the case of Sp^{3+} it is necessary to include ionic correlation effects, but this could be accomplished by modeling the ligands as hard spheres. These results imply that DNA condensation in the presence of polyamines is largely governed by electrostatic interactions. This is in accordance with the observation that condensation is determined by the total charge neutralization of the DNA, rather than by the binding of the multivalent cation *per se*.[1,2]

ACKNOWLEDGMENTS

We acknowledge the Institute Laue-Langevin in providing the neutron research facilities. R. May and I. Grillo are thanked for assistance during the scattering experiments. J. vdM. has benefitted from discussions with C. F. Anderson, M. T. Record, Jr., I. Rouzina, and V. A. Bloomfield. The Netherlands Organization for Scientific Research (NWO) is thanked for a travel grant. L. B. B. wishes to acknowledge an internal grant through FIPI, University of Puerto Rico.

APPENDIX: PARTIAL STRUCTURE FACTORS IN THE CELL MODEL

The rodlike polyion structure can be recognized in Eq. (3) by replacing the integral over $\vec{r}$ in the total volume V into integrals relative to the center of mass of the rod and then sum over all rods. The identical rod carries the label l and its orientation and center of mass are denoted by $\vec{\omega}$ and $\vec{l}$, respectively. The position relative to the center of mass is $\vec{r}_l$ and $\vec{r}=\vec{l}+\vec{r}_l$. With these definitions, the structure factors take the form[6]

$$S_{ij}(q)=\frac{1}{V\rho_L N_i N_j}\left\langle \sum_{ll'} \exp(-i\vec{q}\cdot(\vec{l}-\vec{l}\,')) \times \int_{V_{\text{cell}}} d\vec{r}_l \exp(-i\vec{q}\cdot\vec{r}_l)\rho_i(\vec{r}_l) \times \int_{V_{\text{cell}}} d\vec{r}_{l'} \exp(i\vec{q}\cdot\vec{r}_{l'})\rho_j(\vec{r}_{l'})\right\rangle \tag{A1}$$

and the integrals have to be done over $\vec{r}_l$ in the cell volume V_{cell}. The brackets denote an average over rod orientation and inter-rod separation. The summation runs over all cell pairs ($\vec{l}\neq\vec{l}\,'$) and single cells ($\vec{l}=\vec{l}\,'$).

For a uniform longitudinal monomer and counterion distribution the integral in the cell volume V_{cell} can be factorized into two terms[11]

$$\frac{1}{N_i}\int_{V_{\text{cell}}} d\vec{r}_l \exp(-i\vec{q}\cdot\vec{r}_l)\rho_i(\vec{r}_l) = \frac{\sin(q\mu L/2)}{q\mu L/2}\int_0^{r_{\text{cell}}} dr\, 2\pi r\, J_0(qr\sqrt{1-\mu^2})\,\rho_i(r). \tag{A2}$$

Here, J_0 is the zero order Bessel function of the first kind and μ is related to the rod orientation according to the inproduct $\mu=\vec{q}\cdot\vec{\omega}$. The first term on the right of Eq. (A2) depends on the length L, whereas the second term involves an integral of the radial density profile $\rho_i(r)$. In the case of neutron radiation the condition $qL\gg 1$ is often fulfilled and one essentially probes local structure about the polyion. In this situation, the first term is approximately zero unless $\mu=0$. Accordingly, to a good approximation, the rod orientation μ dependence of the second radial term can be neglected and takes the form

$$a_i(q)=\int_0^{r_{\text{cell}}} dr\, 2\pi r\, J_0(qr)\,\rho_i(r). \tag{A3}$$

If the radial density decays close to zero at the cell boundary, the upper integral limit may be replaced by infinity and Eq. (A3) reduces to a Hankel transform.

The factorization of Eq. (A3) into a length L dependent term and a rod orientation independent radial term is particularly important in recognizing certain relations between the different partial structure factors. For DNA, the linear charge density is so high that most counterions are confined to the immediate vicinity of the polyion. The counterion concentration at the cell boundary is much lower than the average concentration and concentration fluctuations are expected to have little effect on the radial counterion density profile and/or its Hankel transform Eq. (A3). If the radial profiles are assumed invariant to fluctuations in inter-rod separation and orientation, Eq. (A1) can be expressed as a product of terms involving the profiles and a term describing the polymer structure (but for rods with vanishing cross section):

$$S_{ij}(q)=S(q)a_i(q)\,a_j(q) \quad (qL\gg 1) \tag{A4}$$

with

$$S(q)=\frac{1}{V\rho_L}\left\langle \sum_{ll'} \exp(-\vec{q}\cdot(\vec{l}-\vec{l}\,')) \times\frac{\sin(q\mu L/2)}{q\mu L/2}\,\frac{\sin(q\mu' L/2)}{q\mu' L/2}\right\rangle. \tag{A5}$$

The summation runs over all rods ($\vec{l}=\vec{l}\,'$) and rod pairs ($\vec{l}\neq\vec{l}\,'$). For correlations within a single cell, the brackets denote an isotropic orientation average and Eqs. (A4) and (A5) take the relatively simple form

$$S_{ij}(q)=\int_0^1 d\mu\left[\frac{\sin(q\mu L/2)}{q\mu L/2}\right]^2 a_i(q)a_j(q) \approx\frac{\pi}{qL}a_i(q)a_j(q) \quad (qL\gg 1,\vec{l}=\vec{l}\,'). \tag{A6}$$

Here, the polymer structure reduces to the limiting form of the scattering function of a rigid rod with vanishing diameter. For strongly charged rods, there is no closed analytical expression available of the inter-rod structure, and, accordingly, the $\vec{l}\neq\vec{l}\,'$ contributions are difficult to evaluate.

[1] V. A. Bloomfield, Curr. Opin. Struct. Biol. **6**, 334 (1996).
[2] V. A. Bloomfield, Biopolymers **44**, 269 (1998).
[3] A. L. Lehninger, *Biochemistry*, second ed. (Worth Publishers, New York, 1970).
[4] C. F. Anderson and M. T. Record, Jr., Annu. Rev. Phys. Chem. **46**, 657 (1995).
[5] A. P. Lyubartsev and L. Nordenskiöld, J. Phys. Chem. B **101**, 4335 (1997).
[6] S. W. Lovesey, *Theory of Neutron Scattering from Condensed Matter*, Vol. 1 (Oxford University Press, Oxford, 1984).
[7] C. F. Wu, S. H. Chen, L. B. Shih, and J. S. Lin, Phys. Rev. Lett. **61**, 645 (1988).
[8] S.-L. Chang, S.-H. Chen, R. L. Rill, and J. S. Lin, J. Phys. Chem. **94**, 8025 (1990).
[9] S.-L. Chang, S.-H. Chen, R. L. Rill, and J. S. Lin, Prog. Colloid Polym. Sci. **84**, 409 (1991).
[10] B. Guilleaume *et al.*, J. Phys.: Condens. Matter (in press).
[11] J. R. C. van der Maarel *et al.*, J. Phys. II **2**, 109 (1992).
[12] J. R. C. van der Maarel *et al.*, Macromolecules **26**, 7295 (1993).
[13] L. C. A. Groot *et al.*, J. Phys. Chem. **98**, 10167 (1994).
[14] K. Kassapidou *et al.*, Macromolecules **30**, 2671 (1997). Correction: *ibid.* **31**, 1704 (1998).
[15] T. Alfrey, Jr., P. W. Berg, and H. Morawetz, J. Polym. Sci. **7**, 543 (1951).
[16] R. M. Fuoss, A. Katchalsky, and S. Lifson, Proc. Natl. Acad. Sci. USA **37**, 579 (1951).
[17] L. B. Bhuiyan, C. W. Outhwaite, and J. R. C. van der Maarel, Physica A **231**, 295 (1996).
[18] A. Katchalsky, Pure Appl. Chem. **26**, 327 (1971).
[19] T. Das, D. Bratko, L. B. Bhuiyan, and C. W. Outhwaite, J. Phys. Chem. **99**, 410 (1995).
[20] T. Das, D. Bratko, L. B. Bhuiyan, and C. W. Outhwaite, J. Chem. Phys. **107**, 9197 (1997).
[21] This definition differs from previous work, where the structure factors were normalized to the number of nucleotides per fragment. See, e.g., G. Jannink and J. R. C. van der Maarel, Biophys. Chem. **41**, 15 (1991).
[22] Matlab numeric computation software; The Math Works, Natick, MA.
[23] L. Wang, M. Ferrari, and V. A. Bloomfield, Bio Techniques **9**, 24 (1990).
[24] T. Nicolai, L. van Dijk, J. A. P. P. van Dijk, and J. A. M. Smit, J. Chromatogr. **389**, 286 (1987).
[25] D. C. Liebe and J. E. Stuehr, Biopolymers **11**, 167 (1972).
[26] B. Jacrot, Rep. Prog. Phys. **39**, 911 (1976).
[27] J. R. C. van der Maarel and K. Kassapidou, Macromolecules **31**, 5734 (1998).
[28] T. Norisuye, H. Murakama, and H. Fujita, Macromolecules **11**, 966 (1978).
[29] J. L. Finney and J. Turner, Faraday Discuss. Chem. Soc. **85**, 125 (1988).
[30] J.-P. Hansen and I. R. McDonald, *Theory of Simple Liquids*, second ed. (Academic, London, 1986).
[31] The prefactors in the charge structure factor related to the valence are set to unity, because the individual partial structure factors are already normalized.
[32] F. H. Stillinger and R. Lovett, J. Chem. Phys. **49**, 1991 (1968).
[33] J. R. C. van der Maarel, M. Mandel, and G. Jannink, Europhys. Lett. **20**, 607 (1992).
[34] J. R. C. van der Maarel, Biophys. J. **76**, 2673 (1998).